

Emil Vassilev Stanev · Jörg-Olaf Wolff ·  
Gerold Brink-Spalink

## On the sensitivity of the sedimentary system in the East Frisian Wadden Sea to sea-level rise and wave-induced bed shear stress

Received: 28 January 2005 / Accepted: 13 January 2006 / Published online: 30 March 2006  
© Springer-Verlag 2006

**Abstract** The paper addresses the individual and collective contribution of different forcing factors (tides, wind waves, and sea-level rise) to the dynamics of sediment in coastal areas. The results are obtained from simulations with the General Estuarine Transport Model coupled with a sediment transport model. The wave-induced bed shear stress is formulated using a simple model based on the concept that the turbulent kinetic energy (TKE) associated with wind waves is a function of orbital velocity, the latter depending on the wave height and water depth. A theory is presented explaining the controls of sediment dynamics by the TKE produced by tides and wind waves. Several scenarios were developed aiming at revealing possible trends resulting from realistic (observed or expected) changes in sea level and wave magnitude. The simulations demonstrate that these changes not only influence the concentration of sediment, which is very sensitive to the magnitude of the external forcing, but also the temporal variability patterns. The joint effect of tides and wave-induced bed shear stress revealed by the comparison between theoretical results and simulations is well pronounced. The intercomparison between different scenarios demonstrates that the spatial patterns of erosion and deposition are very sensitive to the magnitude of wind waves and sea-level rise. Under a changing climate, forcing the horizontal distribution of sediments adjusts mainly through a change in the balance of export and import of sediment from the intertidal basins. The strongest signal associated with this adjustment is simulated North of the barrier islands where the evolution of sedimentation gives an integrated picture of the processes in tidal basins.

**Keywords** Sediment transport · Numerical modeling · Wind waves · Sea-level rise · Climate change

---

### Introduction

The sedimentary systems in many near coastal areas are strongly coupled with the water dynamics, one illustration is the East Frisian Wadden Sea where physical impacts control coastal erosion and shoreline change through sediment movement. Thus, beaches, barrier islands, bottom profile, and sediment types are adjusted to different forcings: astronomical (tides), atmospheric (wind and wave climate), open ocean (mean sea level, currents, and thermohaline fields), and coastal (fresh water flux). Among the above mentioned forcing factors, signals from the atmosphere and open ocean seem to be the most important ones that will be affected by global climate change. As shown by Forbes et al. (1997) temporal variation in storminess and wind climate can produce significant coastal adjustments. Some studies addressing the potential changes associated with sea-level rise and wave climate (e.g., Komar and Enfield 1987; Nicholls 1998) suggest that the tidal and wind wave impact is expected to extend further inland, making general erosion of sandy shores more likely. According to the idealized model of Bruun (1962), the horizontal shoreline recession  $\Delta x$  required to maintain an equilibrium shore profile under a sea-level rise of  $\Delta z$  can be approximated by  $\Delta x = \frac{l}{h}$  where  $h$  is the maximum depth of exchange of sediment between the nearshore and offshore and  $l$  is the length of the profile from the shoreline to that depth. However, changes cannot be expected to be uniform as assumed in the above model (the Bruun Rule) and local processes controlling the sediment supply may modify these tendencies. Therefore, developing a further understanding of the dynamics of individual coastal systems is desirable.

One difficult problem arises from the fact that changes in the coastal morphometry have small scales (which necessitates us to use small time steps in the models) but at the same time are very slow, which requires long

---

*Responsible editor:* Alejandro J. Souza

---

E. V. Stanev (✉) · J.-O. Wolff · G. Brink-Spalink  
Institute for Chemistry and Biology of the Sea (ICBM),  
University of Oldenburg,  
Postfach 2503,  
26111 Oldenburg, Germany  
e-mail: e.stanev@icbm.de  
Tel.: +49-441-7984061  
Fax: +49-441-7983404

integration times. An illustration of the long-term change in the bed load transport in the North Sea is provided by van der Molen and de Swart (2001) who focused on the contribution of wind waves. Their model is applied to paleoconditions during the Holocene demonstrating that the sand transport mode changed from dominantly suspended transport (before 6,000 years) to dominantly bed load transport because of changing water depth.

The prediction of further changes in a coastal system crucially depends on a thorough understanding of the physical processes acting in the system. We believe that there is a lack of understanding of these fundamental processes. The major problems to be solved include the response to external forcing and the adjustment of the sedimentary system to the new forcing. This is a complex problem and simple conceptual models based solely on sea-level rise and one-dimensional equilibrium bottom profiles are of limited use. The conclusion of Kaplin and Selivanov (1995) that the applicability of the Bruun Rule (Bruun 1962) will diminish under possible future acceleration of sea-level rise is only one among many other concerns about how uncertain the present day predictions could be. The responses of the coastal systems are not easily measurable and attributing different response types to specific forcing is another, still inadequately addressed, problem.

The present paper does not aim to address all the above problems but rather focuses on the sensitivity of one sedimentary system to different forcing. We will limit our scope here to some theoretical issues, elucidation of consequences of some processes, and simulations with realistic 3-D models. In this context, we note that so far there are a number of studies addressing the sensitivity of the response of sedimentary systems to climate change, but not many of them are based on 3-D modeling. The second important point is that there are a number of numerical studies addressing the individual contribution of different properties of forcing on tidal dynamics. For instance, Davies and Lawrence (1994) address the influence of wind and wind-wave turbulence on tidal currents and Friedrichs et al. (1990) address the impact of relative sea-level rise on the evolution of shallow estuaries. However, there is still a lack of theoretical understanding on the individual and collective contribution of different external forcing in the field of sediment dynamics. This is the major interest of the present study, in particular in its aspects addressing one specific region, the one of the Wadden Sea. Compared to our previous study for the same region [E. V. Stanev et al., submitted for publication (SBW)], which was focused on the interplay between transport and turbulence, the present one addresses the response of sedimentary system to changes of external forcing (tides, sea-level rise, and magnitude of wind waves). Because (1) the response to changing magnitude of wind waves is addressed here using a simple parameterization of wind-wave induced bottom stress (without coupling a circulation model with a complex wind-wave model), (2) the numerical integrations are carried out for short periods, and (3) the morphodynamics is not addressed, the present study is regarded as a sensitivity analysis, rather than as a realistic impact study.

The paper is structured as follows. We first describe in Section 2 the basic characteristics of the East Frisian Wadden Sea. The numerical model is described in Section 3, followed in Section 4 by an analysis of circulation and turbulence and the analysis of the individual contribution of different forcing mechanisms establishing the sedimentation in the Wadden Sea. The relevance of the results to climate change problems is also addressed in Section 4, followed by conclusions.

## The East Frisian Wadden Sea

The East Frisian Wadden Sea consists of several tidal basins between barrier islands and the coast (Fig. 1). The physical balances in this mesotidal area tend to locally establish an asymmetry in response to periodic tidal forcing [Stanev et al. 2003a, (SFW)], which minimizes the net export of sediment from the system. As in many other basins of this type, the regime of erosion and deposition shapes the equilibrium bottom profile, which morphodynamically adjusts to the rate of sea-level change (Roberts et al. 2000). A number of observations and results of numerical simulations of the circulation in the Wadden Sea were presented by Stanev et al. (2003b) (SWBBF) therefore, we will give below only a very brief presentation of the physical controls and the sediment dynamics.

The water exchange during one tidal period between the North Sea and individual backbarrier basins varies from  $170 \times 10^6 \text{ m}^3$  to  $40 \times 10^6 \text{ m}^3$ . The above numbers compare well with the tidal prisms. The circulation is dominated by westward transport during ebb and eastward transport during flood. It was demonstrated by SWBBF that while the transport through the inlets is mainly controlled by the



**Fig. 1** The German Bight and the model area (in the red rectangle frame). The gray colors in the near-coastal zone give approximately the areas of the tidal flats (Landsat 5/TMAP, processed by GKSS)

amplitude of the tidal oscillations, the along-shore circulation and the circulation in the inter-tidal areas are controlled by the spatial properties of the forcing signal.

The maximum ebb velocity is observed in the tidal channels shortly before the rate of sea-level fall reaches its maximum. However, the maximum flood velocity is delayed by  $\sim 2$  h with respect to the maximum rate of sea-level rise. This asymmetry is due to the hypsometric control of basins with time-variable horizontal area (SFW).

The turbulent kinetic energy (TKE) is one of the main drivers of the dynamics of suspended particulate matter (SPM). The absolute maxima of TKE driven by tidal forcing only are observed in the tidal inlets and their funnel-like extensions (the regions of the tidal deltas North of the inlets). The minima are in the backbarrier area coinciding approximately with the watersheds separating the individual basins. During most of the time, the entire water column shows a high level of turbulence. Only during slack water (duration of  $\sim 1$  h) the velocity reduces drastically and the level of turbulence diminishes, which enables the deposition of sediment.

The complex temporal and spatial patterns of TKE contribute to the formation of complex friction properties in the model area, which have a number of practical consequences, in particular, the physical control of sediment transport. Up to 7,200 tons of mud and 4,300 tons of sand are moved in and out of the tidal channel of Otzumer Balje (Fig. 2) over one tidal cycle (Santamarina Cuneo and Flemming 2000). It is noteworthy that during slack, water concentrations of SPM reach about 30% of the maximum concentration, while for sand, this number is less than 5 (Santamarina Cuneo and Flemming 2000). Contrary to the sand, which is very sensitive to the level of TKE, the dynamics of SPM, which is the major subject of the present study is strongly affected by the tidal excursions.

Changes in wave or storm patterns may occur under climate change (Schubert et al. 1998). A number of observations and climate change experiments for the 20th century suggest that the storm and wave climate in the North Sea has undergone significant variations on time scales of decades (WASA Group 1998). It is postulated by

Flemming (2002) that sea-level rise creates a sediment deficit in the tidal basins and that the expected morphodynamic response affects the distance between the barrier islands and the coast. The reason for this expectation is based on the fact that the coastal protection systems (dikes) would inhibit natural island dynamics because the tidal signal cannot propagate further inland. The expected increase of energy in the tidal basins would lead to an increased erosion. Without sufficient supply of sediment, the tidal prism would increase and the islands will displace closer to the coast (1 km for sea-level rise of 1 m; Flemming 2002).

Another mechanism forcing the sediment dynamics could be the temperature dependence of kinematic viscosity, which controls the settling velocity (Krögel and Flemming 1998). During summer, viscosity is lower, sinking velocity increases, the mobility of sediment decreases, thus the tidal flats are more stable. The dependence of the sedimentary system on the dynamics (and the induced morphodynamic change) is more pronounced in winter when both meteorological forcing is stronger and sinking is reduced by the low temperatures.

One proof that the morphodynamics of the East Frisian Wadden Sea is very sensitive to various forcing is that land reclamation since 1,300 A.D. resulted in a progressive increase of the length of barrier islands (Flemming and Davis 1994). The tidal flats in the North Frisian Wadden Sea almost disappeared between 1,300 A.D. and the present and the Sylt-Rømø tidal basin almost lost its tidal flats.

The quantification of all the above problems would need much effort. In the present study, we will only focus on the sensitivity of the sediment system to the part of the forcing factors acting in the Wadden Sea.

## The numerical model

### The circulation model

The present work uses results of numerical simulations with the General Estuarine Transport Model (GETM)

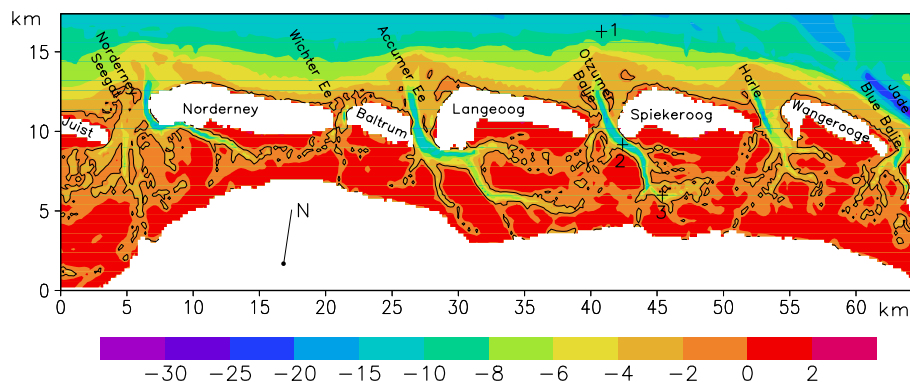


**Fig. 2** Topography of the East Frisian Wadden Sea. The plotted area corresponds to the red frame in Fig. 1. The *isobaths* are represented as *negative numbers* (m) below the mean sea level. The *arrow* giving the direction to the North demonstrates that the model

area is rotated, which is done to reduce the size of model grid. The *contour line* makes possible to distinguish between wet areas and the ones that are prone to drying. Some results of the simulations are discussed for the locations numbered 1, 2, and 3 in the plot

coupled with a sediment transport module. GETM is a 3-D primitive equation numerical model [Burchard and Bolding 2002 (BB)] in which the momentum and continuity equations are supplemented by a pair of equations describing the time evolution of the TKE ( $k$ ) and the eddy dissipation rate ( $\varepsilon$ ).

$$\frac{\partial k}{\partial t} - \frac{\partial}{\partial z} \left( \frac{\nu_t}{\sigma_k} \frac{\partial k}{\partial z} \right) = P - \varepsilon, \quad (1)$$

$$\frac{\partial \varepsilon}{\partial t} - \frac{\partial}{\partial z} \left( \frac{\nu_t}{\sigma_\varepsilon} \frac{\partial \varepsilon}{\partial z} \right) = \frac{\varepsilon}{k} (c_1 P - c_2 \varepsilon), \quad (2)$$

where

$$\nu_t = c_\mu^A \frac{k^2}{\varepsilon} \quad (3)$$

is the eddy viscosity,  $\sigma_k$  and  $\sigma_\varepsilon$  are the turbulent Schmidt numbers,  $c_1 = 1.44$ ,  $c_2 = 1.92$ , and  $c_\mu = 0.56$  (see Rodi 1980; BB; SWBBF).

The vertical shear production  $P$  is a function of the shear frequency  $S$ :

$$P = \nu_t S^2 \quad (4)$$

with

$$S^2 = \left( \frac{\partial u}{\partial z} \right)^2 + \left( \frac{\partial v}{\partial z} \right)^2. \quad (5)$$

A particular feature of GETM is its ability to adequately treat the dynamics in deep inlets, channels, and the tidal flats, the latter falling dry during part of the tidal period. This is achieved by introducing a “drying corrector,” which reduces the influence of some terms in the momentum equations in situations of very thin fluid coverage on the tidal flats. In GETM, a parameter  $\gamma$  is introduced in the hydrodynamical equations, which equals unity in regions where a critical water depth  $D_{crit}$  is exceeded and which approaches zero when the thickness of the water column  $D = h + \zeta$  tends to a minimum value  $D_{min}$ :

$$\gamma = \min \left( 1, \frac{D - D_{min}}{D_{crit} - D_{min}} \right), \quad (6)$$

where  $h$  is the local depth (constant in time) taken as the bottom depth below mean sea level. The minimum allowable thickness  $D_{min}$  of the water column is 2 cm and the critical thickness  $D_{crit}$  is 10 cm (BB and SWBBF). For a water depth greater than 10 cm ( $D \geq D_{crit}$  and  $\gamma = 1$ ), the full physics are included. In the range between critical and minimal thickness (between 10

and 2 cm), the model physics are gradually switched toward friction domination, i.e., by reducing the effects of horizontal advection and Coriolis acceleration and varying the vertical eddy viscosity coefficient according to

$$A_V = \nu_t + (1 - \gamma)\nu_b, \quad (7)$$

where  $\nu_b = 1.8 \times 10^{-6} m^2 s^{-1}$  is a constant background viscosity.

The subgrid scale parameterizations are of utmost importance for the sediment transport and the analysis of simulations by SWBBF demonstrates that the general characteristics of turbulence in the bottom boundary layer are consistent with the requirements formulated by Dyer and Soulsby (1988) for correct prediction of sediment transport rates. The first of them is the logarithmic velocity profile

$$\frac{u}{u_*^b} = \frac{1}{\kappa} \ln \left( \frac{z + z_0}{z_0} \right), \quad (8)$$

where  $u_*^b = \sqrt{\tau_b / \rho_0}$  is the friction velocity at the sea floor,  $\tau_b = \nu_t \rho_0 (\partial u / \partial z)$  is the bed shear-stress,  $\rho_0$  is the water density, and  $z_0$  is the bottom roughness length.

The second requirement, which is the parabolic-like distribution of  $\nu_t$

$$\nu_t = k u_*^b (z + z_0) \left( 1 - \frac{z}{D} \right) \quad (9)$$

is also fulfilled (SWBBF).

We represent the bed shear stress as a sum of two terms (Grant and Madsen 1979; Signell et al. 1990; Davies and Lawrence 1994):

$$\tau_b = \tau_b^t + \tau_b^w, \quad (10)$$

where the first term is due to tidal dynamics (index “t”), and the second one is due to wind waves (index “w”). The contribution of the wind waves to sediment dynamics is based on a simple model assuming that the TKE associated with wave-induced bed shear stress is a function of the wave height and depth. Because this concept is applied only when computing TKE and no explicit waves are included in the model, we do not have a coupling between wind-wave model and circulation model, but rather, a simple parameterization of turbulence. A similar approach was earlier used by Davies and Lawrence (1994) to enhance bottom friction in a 3-D numerical model for specific wave periods and magnitudes and by Souza and Simpson (1997) when studying stratification in coastal waters modified by wind waves.

The bed shear stress can be described (like in steady flows) as proportional to the second power of the orbital velocity (Jonsson 1966). Based on this concept, Le Hir et



al. (2000) found for the shallow water approximation of the orbital velocity, the following expression

$$\tau_b^w = \frac{\rho g f_w H^2}{8 h}, \quad (11)$$

which is used by Roberts et al. (2000) to study the impact of wave-induced bed shear stress on the equilibrium bottom profile. In Eq. 11  $H$  is the wave height and  $f_w$  is the friction factor. Assuming a linear relationship between maximum wave height and local depth, Eq. 11 is modified by Le Hir et al. (2000) as

$$\tau_b^w = \frac{\rho g f_w}{8} \frac{[\min(H_i, (H/h)_{lim} h)]^2}{h}, \quad (12)$$

where  $H_i$  is the incident wave height. The value 0.8 is usually taken as a classical value for  $(H/h)_{lim}$  that is for wave breaking. However, Le Hir et al. (2000) found that for gentle slopes, dissipation becomes dominant and  $H$  tends to a constant proportion of the water depth, whatever the incident wave height is. This proportion gives the maximum wave height such that a tidal flat can experience at a given water depth. For the mudflats studied by Le Hir et al. (2000),  $(H/h)_{lim} = 0.15$ . Furthermore, these authors claim that this value is dependent on the slope of tidal flats. The concept about the control of water depth on the bed shear stress is illustrated in Fig. 3. The conceptual model suggests that erosion will be enhanced in the intermediate depth range where the depth is still large enough to allow high waves (waves with large enough magnitudes, which could substantially affect bed shear stress). Outside this range (deep ocean or very shallow depth), either the level of turbulence is low because of the large depths or the wave height is small because of the small depth. The friction coefficient is taken as  $f_w = 0.005$  and justifications for choosing this number are given in Section 3.4 and in Appendix 1.

Eq. 11 is valid for shallow water waves, thus it does not account for a number of processes associated with real waves. To fully account for the complex wind-waves dynamics, true coupling between circulation and wind wave models is needed, which is beyond the scope of this

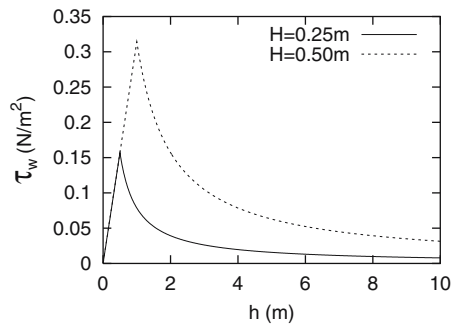


Fig. 3 The bed shear stress as a function of depth  $h$  (Eq. 11)

paper. Here, we just extend the circulation model introducing the above parameterization of wave-induced bed shear stress.

Some of the subgrid parameterizations could depend on the vertical discretization, as is the case with the bed shear stress. In the model, we cannot simply set the lower-most velocity to zero. This would be physically correct for a point directly at the bed, but the lack of resolution in some locations precludes this possibility. To solve that problem, we assume that the lower-most grid box is fully submerged within the logarithmic boundary layer. This does not mean that we directly trigger a log-layer in the whole water column, but only that

$$u_1 = \frac{u_*^b}{\kappa} \ln\left(\frac{0.5h_1 + z_0}{z_0}\right) \quad (13)$$

where  $h_1$ ,  $u_1$  are the thickness and velocity of the deepest box, respectively.

The first application of this model to the area of our study is described by SWBBF and we refer to this paper for more details about the model presentation, its set-up and forcing, and for results of simulations and model validations against observations.

#### Sediment transport model

The sediment transport model uses a standard diffusion–advection equation for sediment concentration  $c$ ,

$$\frac{\partial c}{\partial t} + u \frac{\partial c}{\partial x} + v \frac{\partial c}{\partial y} + w \frac{\partial c}{\partial z} = \frac{\partial}{\partial z} \left( \nu'_t \frac{\partial c}{\partial z} \right) + \frac{\partial}{\partial z} (w_s c), \quad (14)$$

which is on line coupled with the dynamical model. In the above equation,  $u$ ,  $v$ , and  $w$  are the velocity components,  $w_s$  is the settling velocity of the sediment in suspension, and  $\nu'_t$  is the coefficient of turbulent diffusivity. We consider mud of a grain size of  $d = 63 \mu\text{m}$ . Experiments have shown an exponential increase of the settling velocity with the sediment concentration (van Leussen 1988), which is expressed by the formula

$$w_s = k_s c_{nd}^{m_s}, \quad (15)$$

where  $c_{nd} = \frac{c}{c_{un}}$  is a nondimensional concentration of the grain size in question,  $C_{nd} = 1 \text{ kgm}^{-3}$ , and  $k_s$  and  $m_s$  are empirical constants. These are chosen to be  $k_s = 0.017 \text{ ms}^{-1}$  and  $m_s = 1.33$ , in agreement with the measurements summarized in van Leussen (1988).

The sediment flux at the sea bed

$$\left( A_V \frac{\partial c}{\partial z} + w_s c \right)_{z=-H} = E - D, \quad (16)$$

which is the bottom boundary condition of Eq. 14 is based on well-known parameterizations of deposition and erosion rates  $D$  and  $E$ . The deposition rate given by Einstein and Krone (1962) is

$$D = w_s c_b \left(1 - \frac{\tau_b}{\tau_d}\right), \quad (17)$$

where  $c_b$  is the SPM concentration near the bottom,  $\tau_b$  is the bed shear stress, and  $\tau_d$  is the critical shear stress for deposition.

The erosion rate is computed using the formula of Partheniades (1965):

$$E = \alpha M_e \left(\frac{\tau_b}{\tau_e} - 1\right), \quad (18)$$

where  $M_e$  is an empirical constant giving the erosion rate at twice the critical shear stress for erosion. The parameter  $\alpha$  specifies the fraction of the grain size in question in the bottom sediment and has a value between 0 and 1. The value used for  $M_e$  is  $3.7 \cdot 10^{-6} \text{ kgm}^{-2}\text{s}^{-1}$ . This is somewhat smaller than the values suggested by other authors (e.g., Mehta 1988; Puls and Sündermann 1990; Clarke and Elliot 1998) ranging between  $6 \times 10^{-6}$  and  $4 \times 10^{-3} \text{ kgm}^{-2}\text{s}^{-1}$ , but showed good results in initial model runs.

The critical shear stress for erosion is set constant to  $0.2 \text{ Nm}^{-2}$ . The critical shear stress for deposition is chosen to be equal to that for erosion. That means that either deposition or erosion occurs and no region of transition exists where neither of the two processes are active.

We remind that discrete bottom values of SPM are positioned half a grid box above the bottom, while the turbulent quantities are just at the bottom (Burchard et al. 1999). Therefore, we have to make an assumption about the profile of SPM (as this is the case with velocities, Eq. 13). With the viscosity profile given by Eq. 9, constant  $w_s$  and constant Prandtl number  $Pr = \nu_t/\nu'_t$ , the one-dimen-

sional stationary equation Eq. 14 has a solution in the form of the so-called Rouse profile

$$c = c_0 \left(\frac{D-z}{z} \frac{z_0}{D-z_0}\right)^{\frac{Pr}{B}}, \quad (19)$$

where  $B = \frac{w_s}{ku_*}$  is the Rouse number (see also Burchard et al. 1999). Instead, to use in the deposition term (Eq. 17) the computed sediment value at the first level where we integrate sediment transport equation we account for the above profile by extrapolating the bottom concentration  $c_b$  from the two lowest layers ( $c_b = c_1(c_1/c_2)^q$ ) where  $c_1$  and  $c_2$  are concentrations at depths  $h_1$  and  $h_2$ , correspondingly. Obviously,  $q$  depends on how we resolve the bed layer. It can be easily shown that for equidistant resolution  $q \approx 2$ . This extrapolation is consistent with the Rouse profile and is superior to the linear extrapolation, the latter is very inaccurate in the areas of high bottom gradients.

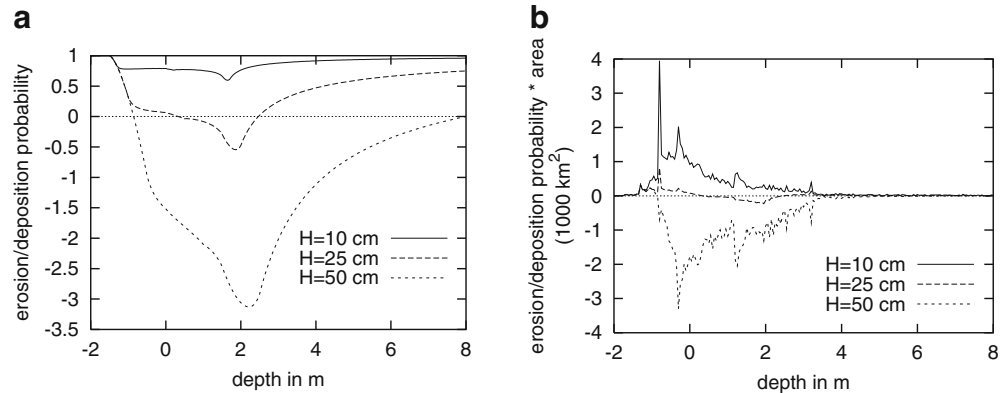
The implications of the parameterization of wave-induced bottom stress (see also Section 4 and Appendix 1) for the sediment dynamics of near coastal areas becomes clear from Fig. 4. The left panel (a) shows the normalized (maximum deposition/erosion =  $\pm 1$ ) probability expressed as integrated over one tidal cycle:

$$\Phi = \frac{1}{T} \int_T \frac{\tau_{d,e} - \tau_b^w}{\tau_{d,e}} dt, \quad (20)$$

(see Eq. 16, 17, and 18). The threshold bed shear stress for erosion and deposition  $\tau_{d,e}$  is  $0.2 \text{ Nm}^{-2}$  and the tidal range was chosen to be 3 m. The right panel (b) shows the same data weighted by the area with which the particular depths occur in the Wadden Sea area (Fig. 2).

In all cases, a net SPM flux due to wind waves is observed in the shallow area. However, depending on the height of wind waves, there is an accumulation trend (for small waves) and erosion trend for large waves. For some

**Fig. 4** Normalized vertical flux of sediment for different wave heights due to waves during one tidal cycle. Values in the *right* panel are weighted by the *hypsometric curve*. Positive and negative numbers on y-axis indicate accumulation and erosion trends, correspondingly



intermediate wave heights, there is a trend of redistribution of the sediment (accumulation in the very shallow area and erosion from the deeper one, which is consistent with the results of Roberts et al. 2000). It is noteworthy that when weighted by the area, the fluxes in Fig. 4b change considerably, compared to the ones in Fig. 4a. The largest fluxes displace toward smaller depths, which results from the fact that depths in the intertidal flats are very small. Depending on the magnitude of wind waves, the fine sediment can either be eroded or deposited. The control of the fluxes by topography gives an idea about possible feedbacks. Under wave action the erosion tends to increase the depth (the negative curve in Fig. 4b). Then the same waves start to propagate on deeper bottom and deposition becomes dominating. Although the above considerations are based on a simple theory, it is obvious that the sedimentary systems may undergo, in the realistic cases, multiple responses shaped by the balance between tides, wind waves, and sea level. This issue is investigated further with the help of a numerical model.

#### The model grid, forcing, and numerical experiments

The horizontal matrix includes  $324 \times 88$  grid-points in the zonal and meridional direction with 200 m steps. In the vertical, the model uses terrain-following coordinates. The vertical discretization consists of ten equidistant layers extending from the bottom  $h$  to the sea surface  $\zeta$ .

The forcing at the open boundaries is taken from the simulations with the operational model of the German Bight provided by the German Weather Service (Dick et al. 2001). The output of the Bundesanstalt für Seeschifffahrt und Hydrographie model incorporates the main elements of the regional circulation, which is the coastal wave associated with the well-known amphidromy at  $\sim (55.5^{\circ} N, 5.5^{\circ} E)$ . The tidal signal crosses the model area from West to East in  $\sim 50$  min. The vertical motion of the sea level at the open boundary and its slope provide the major driving force for the model (the technical details describing the forcing of the regional model are given in SWBBF).

In the present study, we will discuss only the results of simulations for the period October 16 to 18, 2000, which are representative for the general conditions during spring tide (see SWBBF for more details about the results of simulations). The sediment source at the bottom is taken to be inexhaustible everywhere. Effects of erosion or deposition on the bathymetry are not considered in our simulations.

Lateral boundary conditions for SPM are taken to be zero for inflowing water. Outflowing water results in a sediment flux out of the model area of  $u_n c$  where  $u_n$  is the velocity normal to the boundary. In a first run the initial concentration of SPM was set to zero everywhere. The SPM concentration continuously increases and equilibrium is not reached before four tidal periods. Thus, the SPM field after four tidal cycles of a run started with  $c = 0$  was taken as the initial field for all other runs. This method reduces the time of adjustment. The sediment transport

routine is not started until half a tidal period has passed to let the hydrodynamics adjust to the forcing. This avoids a nonrealistic high erosion rate in some areas.

#### Numerical experiments

In the following we discuss the results of several numerical experiments aiming to reveal the sensitivity of the sedimentary system to external forcing. This issue is relevant to the sensitivity of sediment dynamics to global and local climate change. We will further assume that the astronomical forcing (characteristics of tidal oscillations) remains the same, but that the sea level or wave height changes. We therefore carry out the following experiments. The first one is called Control Run (CR) and is forced only by tides at the open boundary of the model. This is essentially the same experiment, which is presented in the study of SBW. In the second experiment, we add to the model forcing wind waves with a height of 25 cm (W25). The third experiment (W50) is the same as the second one, but the height of wind waves is taken as 50 cm. In the fourth experiment we do not include wind waves, but instead assume a sea-level rise (SLR-experiment) of 1 m. In the last experiment (SLRW25) we include both effects: sea-level rise of 1 m and wind waves of 25 cm. When formulating the above experiments we take the same tidal forcing for all experiments. This assumption excludes the change in the North Sea tidal system, which might occur if sea level increases. This issue can become a subject of a separate study.

There are a number of parameterizations of the wave friction factor  $f_w$  (see Jonsson 1966 and the review of Bruun 1978), most of which were not tested over wide areas of the ocean bed. The major difficulty is to find the right “weighting” of different mechanisms contributing to the bed shear stress. The sensitivity experiments analyzed in Appendix 1 show that sediment dynamics are strongly affected by the choice of the wave friction ( $f_w$ ) and wave breaking  $(H/h)_{lim}$  factor.

Because our main purpose in this paper is to reveal the level of sensitivity of the entire sedimentary system to wave-induced bed shear stress, we propose the following pragmatic approach based on the results of recent observations by Santamarina Cuneo and Flemming (2000). During calm weather conditions, the concentration of mud in suspension was approximately the same (about 50–60 mg/l) during peak ebb and peak flood. The concentrations of sand were much smaller. Under windy conditions (northerly winds and 1-m waves), the flood maximum of mud concentrations became about twice the ebb maximum. Under moderate wind conditions, the concentration of sand increased considerably and the sand maximum (also during flood) exceeded the one of the mud. The fact that the mud concentrations do not change much reveals that the erosion by breaking waves in the Southern North Sea is limited by the larger depths.

We carried out several sensitivity experiments with  $(H/h)_{lim} = 0.5$  (see also Appendix 1) in which we changed only  $f_w$  and found out that the simulated concentration in the tidal channels is close to the observed one for  $f_w = 0.005$ . This number is within the ranges proposed in other studies (see Jonsson 1966; Le Hir et al. 2000) and our pragmatic method for estimation of  $f_w$  can be regarded as an indirect method to obtain a bulk value of this parameter in our specific region, which is characterized with a very gentle bottom slope. We admit that our experiments are just sensitivity studies and cannot answer the question about what would be the long-term change in the sedimentary system in the East Frisian Wadden Sea if one or several forcing factors change. In the real case, the response is accompanied by redistribution of sediment on the bed and changing topography (in our study topography does not change). The answer of the fundamental question about long-term changes and their quantification would need further efforts. One extremely difficult problem is to enable at

the same time enough length of integration times and accuracy in the models. We remind here that using simplified numerical models (e.g., 2-D models) could substantially affect the physical resolution of some important processes for the sediment dynamics (SBW).

The setup of the above experiments and the data analysis presented below can give a coarse idea about possible trends and about the joint effects of multiple forcing mechanisms. This is the reason why we focus in Section 4 on the physical interpretations of the response effects.

## Analysis of numerical simulations

### Physical response

We will illustrate below the physical responses using the simulated data of velocity and TKE. As could be expected, adding the effect of wave breaking does not substantially affect the transport patterns (Figs. 5 and 6). This effect adds

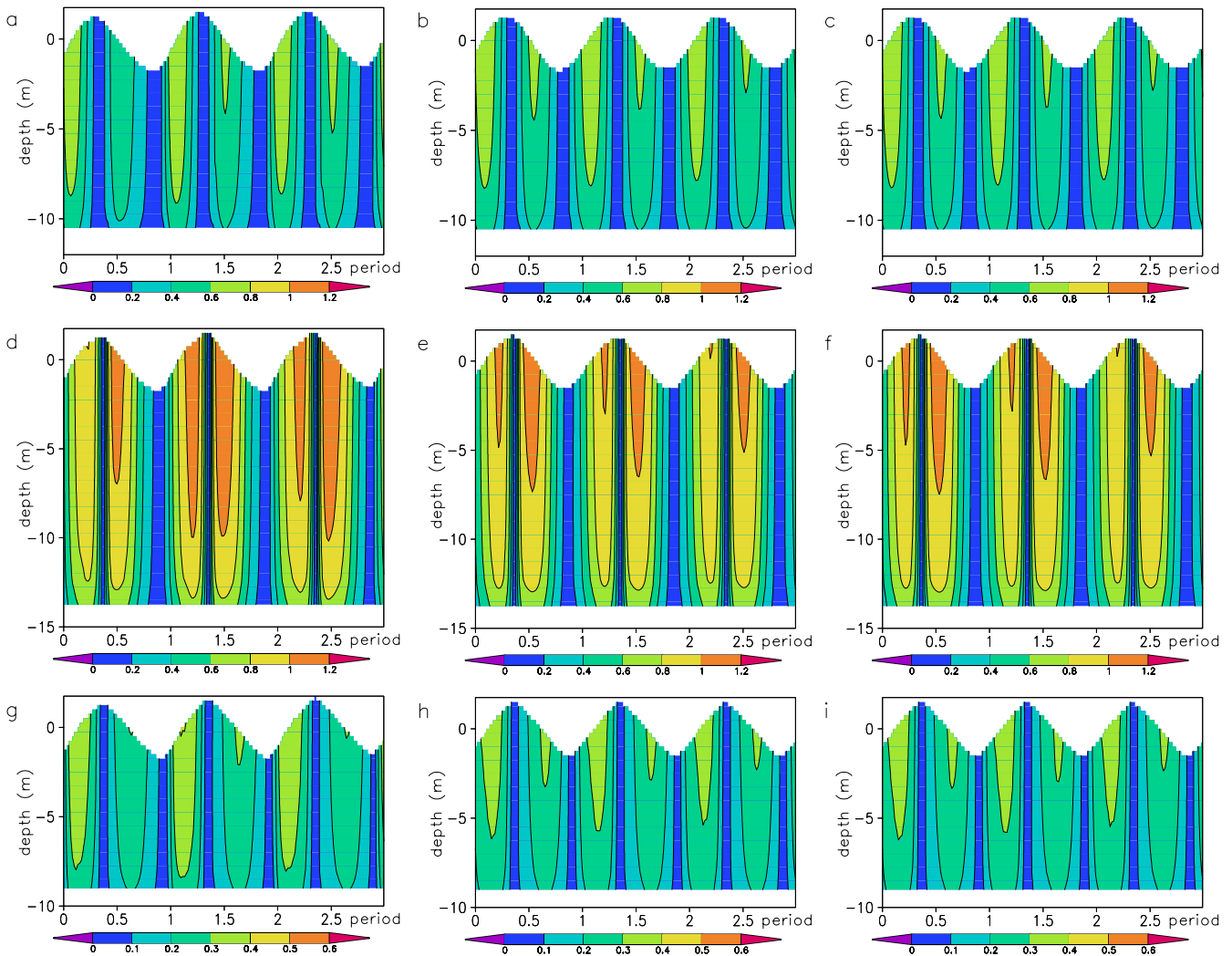


**Fig. 5** Velocity magnitude (in m/s) during three tidal periods in front of the backbarrier islands (a–c), tidal channels (d–f), and tidal basins (g–i). The *first column* (a, d, g) is from experiment CR, the

*second column* (b, e, h) is from W025, and the *third column* (c, f, i) is from W050



some more friction to the dynamical system (located in the area of wave breaking). However, as known from previous studies (SFW), the response of dynamical system to tidal forcing is mostly controlled by the topography (hypso-metry), therefore, the velocity magnitude in W25 and W50 follows approximately the patterns in CR. This result becomes more clear from the curves comparing the temporal variabilities simulated in several experiments (Fig. 7).

Dynamics become very sensitive to sea-level rise (Fig. 6). This is explained by the fact that higher water level would contribute to an increase of the tidal prism because the morphometry in the model does not change. This statement becomes clear from the definition of the excess volume as

$$V = \int_0^{\zeta} A_b(z) dz, \quad (21)$$

where  $A_b$  is the area of tidal basin. Because the dikes along the coast do not allow further propagation of the sea inland,

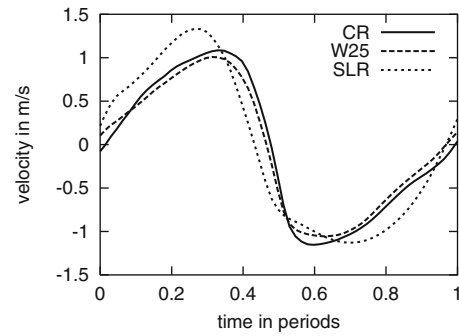


Fig. 7 Temporal evolution of velocity in the tidal channel “Otzumer Balje” in the middle of the water column (see Fig. 2 for the positions)

the area undergoing drying reduces and the mean  $A_b$  increases (tending to the maximum value corresponding to the area encircled by the dike-line). The final result is that the basin area of tidal basins becomes less dependent on the height of sea level and the above integral will increase.

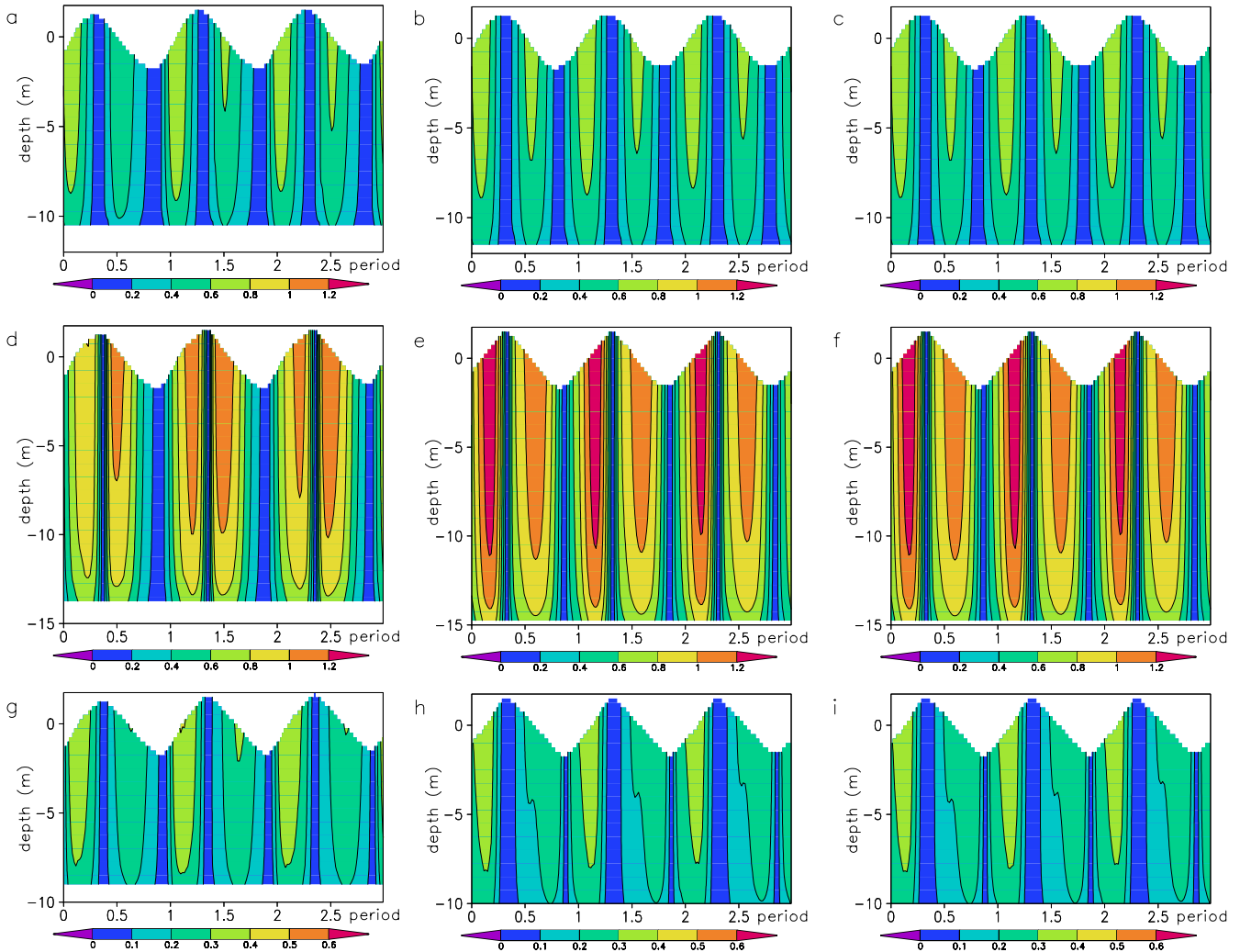


Fig. 6 Velocity magnitude (in m/s) during three tidal periods in front of the backbarrier islands (a–c), tidal channels (d–f), and tidal basins (g–i). The first column (a, d, g) is from experiment CR, the

second column (b, e, h) is from SLR, and the third column (c, f, i) is from SLRW25

More specifically, SLR of 1 m resulted in an increase of the tidal prism of Spiekeroog area from  $127$  to  $188 \times 10^6 \text{m}^3$ . This results in a decrease in ebb-dominated asymmetries because the area undergoing drying gets smaller (see for more details SWBBF and SFW) and as seen in Fig. 6, the maximum flood increases considerably. This effect is well pronounced in the tidal channels, which give an integrated measure of the response of tidal flats to forcing from the open ocean.

The above effects are seen well in Fig. 7 demonstrating that (1) it is the maximum flood in the tidal channels, which is higher in SLR but not the ebb one and (2) the transition between flood and ebb is less steep in SLR than in CR. Both effects contribute to a transition of the sedimentary system from ebb dominance toward flood dominance.

The level of turbulence changes in the model as a result of both wave breaking and sea-level rise (Figs. 8 and 9). Rising sea level does not have a pronounced effect on the TKE north of the barrier islands. In the tidal channels, the time vs depth diagrams inversely follow the evolution of currents (maximum velocity is in the surface layers, maximum TKE in the bottom layers) and the sensitivity

to sea-level rise is strong. In the tidal flats, it takes much longer to establish the flood maximum in SLR than in CR.

The effects of wave breaking are more pronounced in the tidal flats where the maximum flood becomes wider and slightly weaker. In this way, the effect of breaking waves ensures high enough energy for a longer time, thus keeping SPM in the water column. Better insight about the different levels of TKE due to tides and wind waves can be obtained from Fig. 10.

### The response of sediment

The response of the sedimentary system in the East Frisian Wadden Sea to tidal forcing was analyzed by SBW and we refer to this study for more details about the results from experiment CR. Here, we would like to mention that the temporal evolution of SPM north of the barrier islands (Fig. 11a) is shaped by advection of SPM in the tidal channels originating from the inlets and their catchment areas. The relative role of the TKE increases in tidal channels where the SPM shows two maxima associated

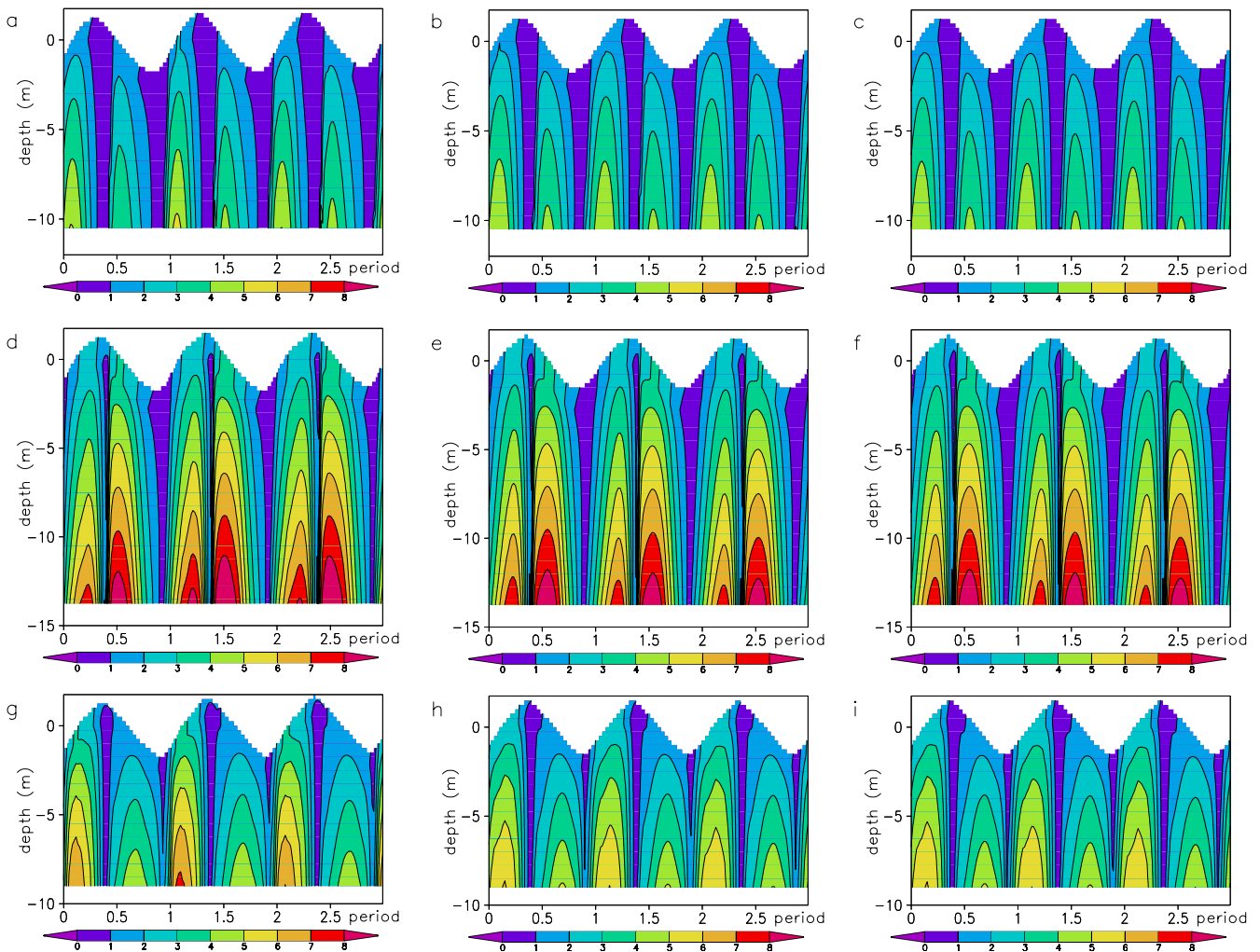


**Fig. 8** TKE (in  $\text{cm}^2/\text{s}^2$ ) during three tidal periods in front of the backbarrier islands (a–c), tidal channels (d–f), and tidal basins (g–i). The first column (a, d, g) is from experiment CR, the second column (b, e, h) is from W025, and the third column (c, f, i) is from W050

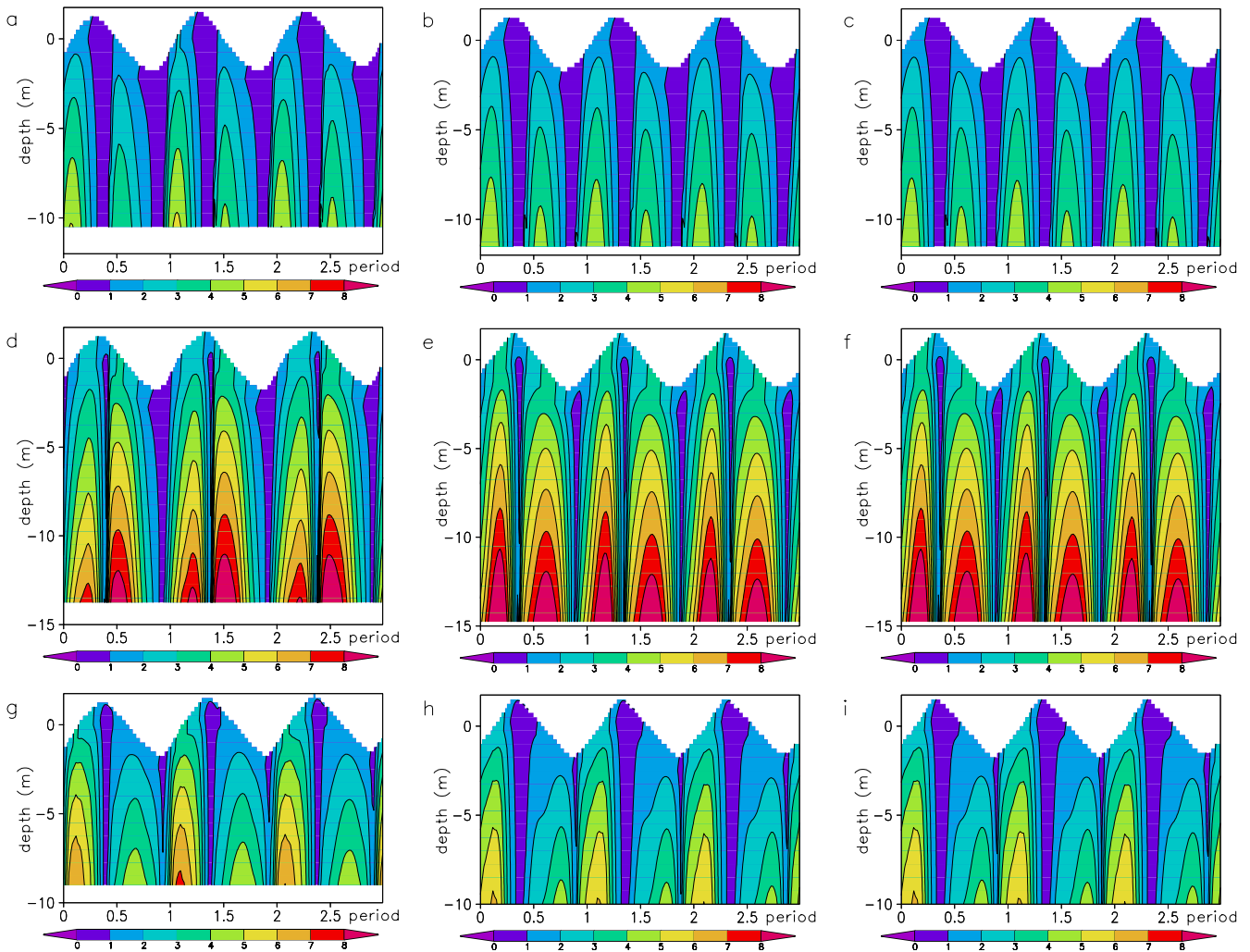


**Fig. 9** TKE (in  $\text{cm}^2/\text{s}^2$ ) during three tidal periods in front of the backbarrier islands (a–c), tidal channels (d–f), and tidal basins (g–i). The first column (a, d, g) is from experiment CR, the second column (b, e, h) is from SLR, and the third column (c, f, i) is from SLRW25

with flood and ebb currents. During the ebb phase, the TKE is higher (Fig. 8d). However, the time variability of SPM differs from the one of TKE, revealing that local models (without advection) would hardly resolve important temporal patterns (see also SBW). In the shallow extensions of the tidal channels (Fig. 11g) the maximum concentration of SPM is simulated during flood, revealing not only that dynamics in the shallow area becomes flood-dominated (Stanev et al. submitted to Cont. Shelf Res.) but also that there is a substantial difference between the sediment response to the tidal signal in the tidal flats and tidal inlets.

Adding 0.25 m wind waves to the model forcing (W25) results in a substantial increase of sediment concentration: about 1.25 times in the North Sea area, 1.35 times in the tidal channels, and 1.24 times in the tidal flats. To enable a comparison between different experiments, we show the results in Fig. 11 and Fig. 12 as anomalies from the mean (the mean value is also given). Only the results in CR are presented in Fig. 11 in concentration units.

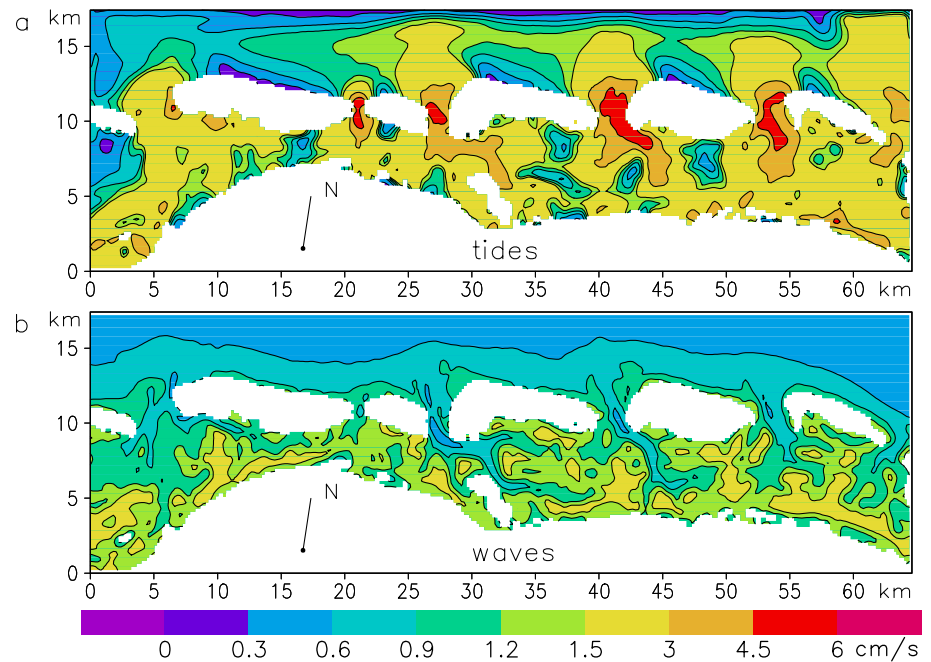
The vertical stratification of SPM is stronger in the case with wave-induced bed shear stress. It is seen from the

comparison between Fig. 11a and b that the sediment maximum (due to the supply of sediments from tidal flats) is stronger and more localized around the time of low water. While the general pattern of variability in the tidal channels does not drastically differ from CR to W25, there are some important qualitative changes: Flood maximum is higher than the ebb one in W25, which is even more pronounced in W50.

It is well known from the observations existing in the Wadden Sea (and elsewhere) that minimum concentrations in tidal inlets appear during low and high water. The single maximum in the tidal flats (Fig. 11g) was explained by SBW as a consequence of the complicated interplay between turbulence and advection. The result is the transition of the system in the tidal basins toward flood dominance (Stanev et al. submitted to Cont. Shelf Res.). Thus, the sediment maximum in the shallow extensions of tidal channels gives one proof of that.

With the present simulations (W25 and W50) we see that there are also higher harmonics in the sediment concentrations on the tidal flats, which is more pronounced in W50.

**Fig. 10** Friction velocity due to tidal forcing (a) and forcing by wind waves (b)



These low water maxima are separated one from another by a local minimum of concentration appearing exactly at low water. These simulations are consistent with the theoretical considerations in Appendix 1 (Fig. 17), explaining the narrow peaks shortly before and just after the low water. The flood peak in Fig. 11g,h, which gives the absolute maximum of the concentration, decreases relatively in W50 (Fig. 11i). Obviously, with the prescribed wave height in W50, it is possible to convert the sedimentary system in the tidal flats into a state dominated by wave breaking. The sea-level rise in SLR tends to decrease the ebb dominated asymmetry. The sediment response, thus demonstrates narrower peaks. In the tidal channels they are stronger during flood, which is opposite to the case in CR. The situation in the tidal flats does not change qualitatively compared to the one in CR. It is noteworthy that the contrast in time increases slightly in SLR.

The simulations in SLRW25 (Fig. 12c,f,i) reveal that the collective contribution of wave-induced bed shear stress and sea-level rise represents approximately a sum of their individual contributions. Therefore, we will not discuss the collective effects in detail. The only important result to mention here is that the sea-level rise tends to reduce the effect of the increased sediment concentrations due to erosion from wind waves by about 15%. The explanation is that the wave breaking in the deep water is less efficient (the water is deeper because dikes make it impossible for the tidal wave to reach very shallow depths). One expectation about the contribution of wave-induced bed shear stress and sea-level rise to the sediment dynamics in the entire region of simulations is given in Fig. 10. The result can be seen in Fig. 13a where we display differential plots between deposition and erosion in some of the simulations. The general conclusion is that in most of the inlets, the sea-level rise leads to an increase of erosion, which is consistent with a number of speculations that sea-

level rise would increase the erosion of sediment from tidal basin. However, the simulations demonstrate that this is true only in part of the tidal basins and, in particular, in the extensions of inlets. On the contrary, the deposition of sediment is enhanced on the tidal flats and the reason for that is that the tidal asymmetry changes. This effect could result in reshaping the morphodynamics because in some areas accumulation of sediment would become possible.

The conclusions about the role of the wind waves are also not trivial. From the bed shear stress shown in Fig. 10 one could expect the trend of erosion of shallow areas and deposition in the deep ones. This expectation is valid for most of the tidal basins in Fig. 13b. However, the pattern of deposition minus erosion (D–E) north of the barrier islands indicates that although everywhere north of the barrier islands the wave-induced bed shear stress is small (Fig. 13b), the trends of deposition minus erosion are characterized by specific spatial patterns. We remind that the direction of propagation of wind waves is not considered here and some differences from the trends in the real system due to increased wind waves are not excluded.

The above analysis motivates the question about the general patterns of erosion and deposition in the Wadden Sea. The fluxes of deposition minus erosion (Fig. 14a) averaged in different depth ranges reveal that under tidal forcing only, almost all depth range is dominated by erosion. The wind action, as explained previously, tends to decrease this negative trend. The major question arising here is about the stability of the sediment system (why is the erosion dominating). Actually, Fig. 14a does not account for the areas of different depth ranges. When weighting the results with the areas, we see that the integral in CR decreases considerably. Shallow areas are subject to accumulation and the deeper ones to erosion. This is another indication that there is no complete equilibrium, but one cannot expect that such equilibrium would be



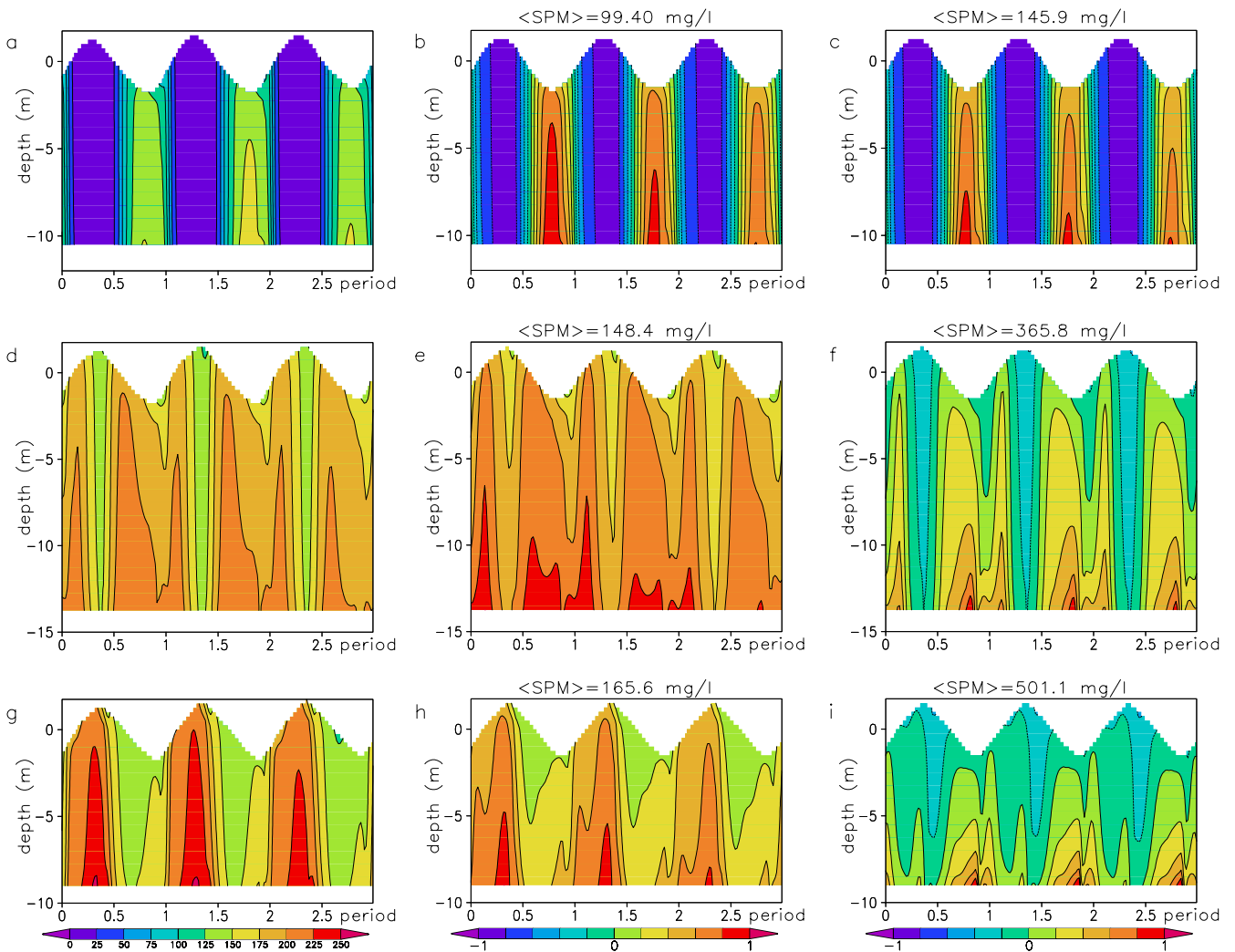


**Fig. 11** SPM concentrations during three tidal periods in front of the backbarrier islands (a–c), tidal channels (d–f), and tidal basins (g–i). The *first column* (a, d, g) is from experiment CR and shows real concentration, the *second column* (b, e, h) is from W025, and

the *third column* (c, f, i) is from W050. The latter diagrams show anomaly of concentration, which is  $-1$  for concentration=0,  $+1$  for the maximum concentration, and  $0$  for the mean concentration (half of maximum; value is given in the plots)

reached without morphodynamic adjustment (we do not account for this process in the present model). By introducing small wave action (W25) the sedimentary system tends to decrease the spatial inhomogeneity between deposition and erosion. Doubling this forcing transforms the system to an eroding system almost everywhere with an approximate rate of about 5 cm/year.

The contribution of dynamics (including sediment dynamics) in shaping the deposition minus erosion is seen from the comparison between theoretical results (Fig. 4) and simulations (Fig. 14). We admit that this comparison is not perfect because of some differences between the theoretical model and the simulations. One of them is that in the numerical model, the bed fluxes are functions of the computed concentration of sediment. Another more important difference is that tidal shear stress is not considered in the theoretical model. The trend of increasing the erosion vs deposition with the increasing wave height persists in both models. However, with small wind waves,

the theoretical model (no advection) gives an enhancement of the deposition in all depth ranges, which is not the case in the numerical simulations. This is another proof of the role played by dynamics and a caveat that using simple models can give only limited information about changes of sedimentary systems under climate change.

## Conclusions

The impact of external forcing on the sedimentary system of the East Frisian Wadden Sea was investigated by using of a 3-D hydrodynamic model combined with a sediment transport model. In particular, a sea-level rise and wave-induced bed shear stress were added to the external forcing in different magnitudes and combinations to reveal their individual and collective impacts.

The simulations showed that a sea-level rise of 1 m results in an increase of the tidal prisms, thus shifting the

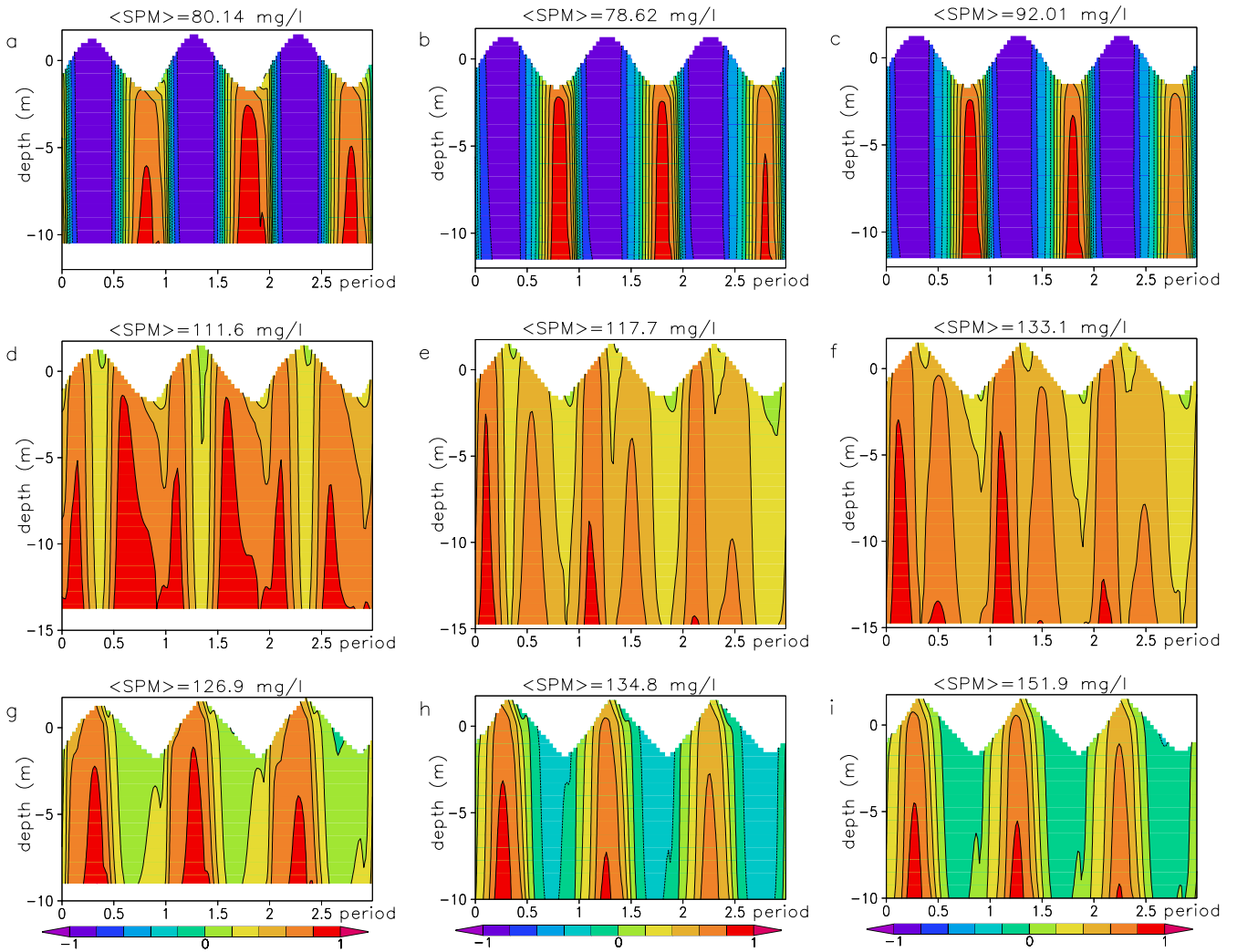


**Fig. 12** SPM concentrations during three tidal periods in front of the backbarrier islands (a–c), tidal channels (d–f), and tidal basins (g–i). The first column (a, d, g) is from experiment CR, the second column (b, e, h) is from SLR, and the third column (c, f, i) is from SLRW25

**Fig. 13** Deposition minus erosion in SLR and CR (a) and W25 and CR (b)

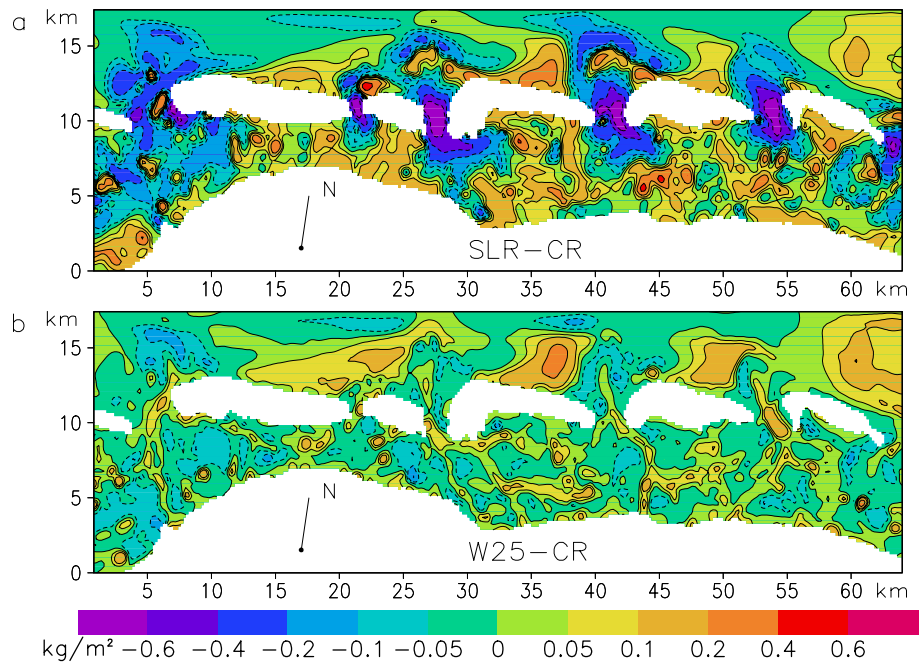
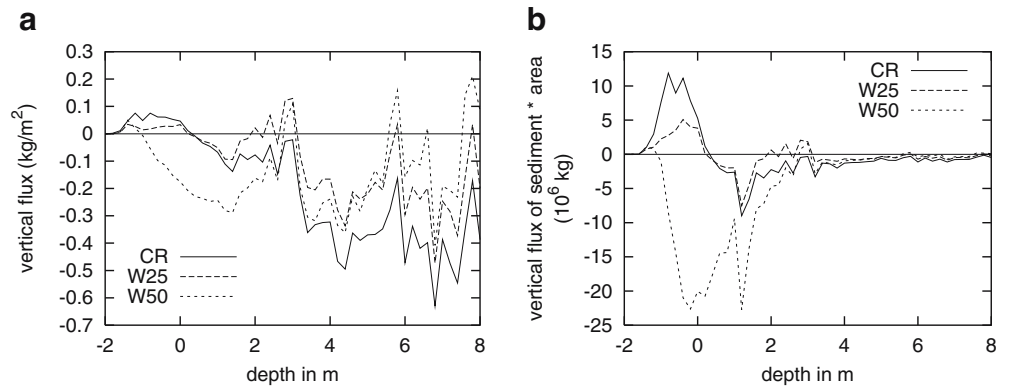


**Fig. 14** Vertical flux of sediment for different wave heights as a function of depth integrated over one tidal cycle. Per unit area (a), integrated over the model area and a depth-interval of 1 m (b)



ebb-dominated asymmetry in the tidal channels toward flood-domination. The maximum flood velocity increases and the level of turbulence, which substantially changes the transport of sediment in the tidal channels, also increases. It is demonstrated that the widely accepted assumption that the sea-level rise would result in an increased erosion is not valid for the entire tidal basin. The changing asymmetry in the tidal response leads to an increased accumulation of sediment on the tidal flats. This result reveals that highly nonlinear and space-dependent response processes are of utmost importance even when applying seemingly simple changes to the forcing.

The concentration of SPM in the water column is higher almost throughout the whole tidal cycle when we add the wave-induced bed shear stress or sea-level rise to the tidal forcing. This applies especially to the cases with wind waves where higher magnitudes result in increased bottom shear stress and higher erosion, thus higher concentrations of sediment.

The horizontal transport is not substantially affected by wave-induced bed shear stress because tidal currents are mainly controlled by the topography and friction. However, qualitative changes are observed in the temporal evolution of the concentration of SPM. The flood maximum increases in the tidal channels and higher harmonics enhance in the tidal flats. The additional concentration peaks support the theoretical considerations also presented in this paper. A sinusoidal tidal wave was applied to a simple topography with a constant slope under the use of depth-dependent wave impact. This also results in a twin peak structure similar to that resulting from the numerical model. Simple theoretical analysis is carried out in Appendix 1 demonstrating that the interplay of tidal range, wave height, and bottom slope can result in either unimodal or bimodal behavior of the bottom shear stress, depending on the ratio between amplitudes. In general, steep slopes and high waves lead to unimodal oscillations of the bottom shear stress and sediment concentration. Weak slopes and small waves give rise to bimodal oscillations.

The impact of wave-induced bed shear stress on sediment dynamics is very pronounced on the tidal flats. In the case of small or no wind waves, there is a general deposition trend. Because the tidal flats cover a large area of the Wadden Sea, the overall sediment budget is clearly positive. With larger wave magnitudes the shallow areas

become subject to erosion, thus reversing the situation. The conclusion is that the sediment balance of tidal flats is very sensitive to changes in the forcing by wind waves.

It is demonstrated that the collective impact of sea-level rise and wave-induced bed shear stress leads to an addition of the corresponding response effects. Therefore, the contribution of waves diminishes when the sea level is higher, which is due to larger depths making the wave breaking a less effective mixing factor. This result holds in systems that cannot extend land wards because of dikes.

## Appendix 1

Here, we will use for the bed shear stress Eq. 10 and, as done in many theoretical studies of the bottom layer, we parameterize  $\tau_b^t$  as

$$\tau_b^t = \rho c_D u^2, \quad (22)$$

where  $u$  is the mean velocity.

We will apply the above equations to an idealized topography with a constant slope  $a = \frac{dh}{dx}$  (Fig. 15). For simplicity, we will assume that  $\zeta = \frac{\zeta}{2} \cos \omega t$  where  $r$  is the tidal range (Fig. 16a), that is we neglect the spatial dependence. As demonstrated by SFW, this assumption is approximately valid over the tidal flats. The volume of water between the location where the depth is  $H_{lw}$  (see Fig. 15) and the movable boundary is

$$V = [x_{lw}(\frac{H_{lw}}{2} + \zeta) + \Delta x \frac{\zeta}{2}] y_0, \quad (23)$$

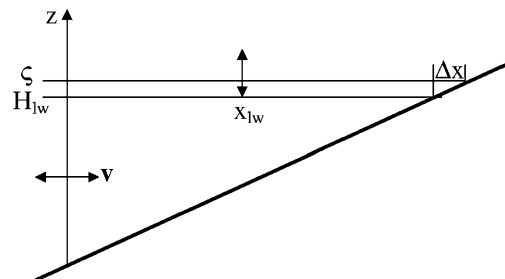
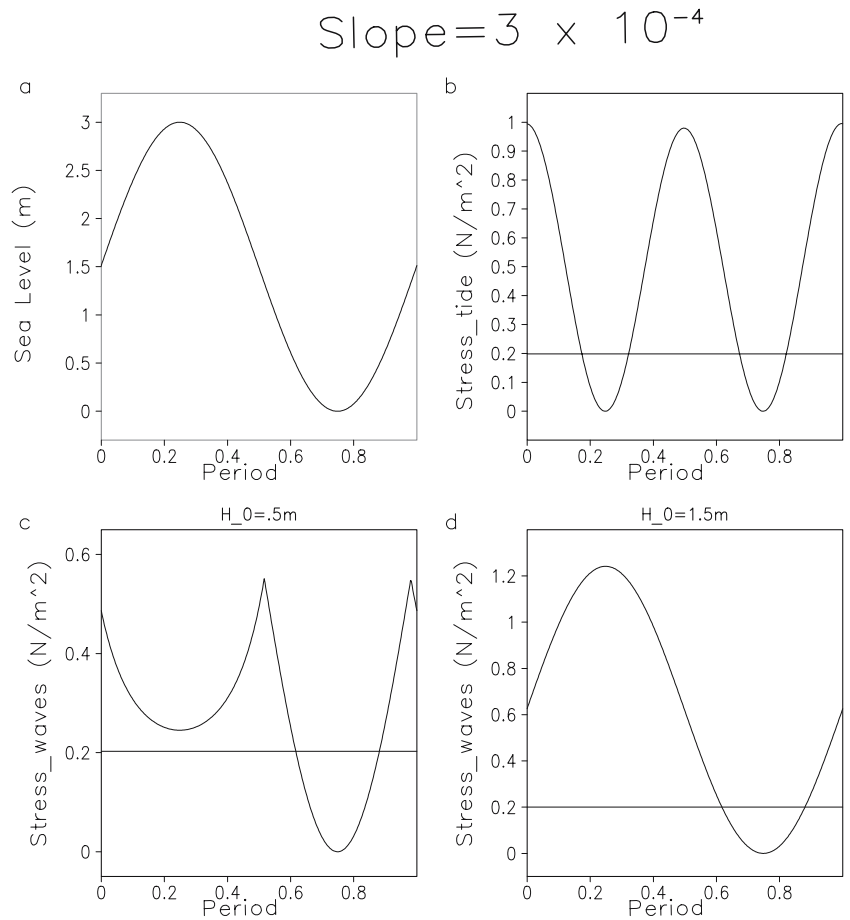


**Fig. 15** The simplified topography

**Fig. 16** Temporal variability during one tidal period of sea level (a), bed shear stress due to tides (b), and bed shear stress due to wind waves (c and d). In this case  $f_w = 0.015$  and the limiting factor  $(H/h)_{lim} = 0.15$ . The horizontal lines at  $0.2Nm^{-2}$  indicates critical shear stress



where  $y_0$  is the extension along the coast of the area,  $x_{lw} = \frac{H_{lw}}{a}$  is the distance between location where the depth is  $H_{lw}$  and the coast,  $\Delta x = \frac{\zeta}{a}$ . The total transport is  $Tr = \frac{dV}{dt} = x \frac{d\zeta}{dt} y_0$  where  $x = \frac{(H_{lw} + \zeta)}{a}$  is the extension of the flooded area. Velocity is computed as  $v = \frac{1}{y_0(H_{lw} + \zeta)} \frac{dV}{dt}$  and

for the given  $\zeta$  is  $v = -\frac{r\omega}{2a} \sin\omega t$ . The corresponding bed shear stress computed from Eq. 22

$$\tau_b^t = \rho c_D \left(\frac{r\omega}{2a}\right)^2 \sin^2 \omega t = \rho c_D \left(\frac{r\omega}{2a}\right)^2 \frac{(1 - \cos 2\omega t)}{2} \quad (24)$$

is shown in Fig. 16b. This is a bimodal oscillation shaped by the maxima of current speed.

**Fig. 17** Temporal variability during one tidal period of bed shear stress due to wind waves. In this case  $f_w = 0.005$  and the limiting factor  $(H/h)_{lim} = 0.5$ . The horizontal lines at  $0.2Nm^{-2}$  indicates critical shear stress

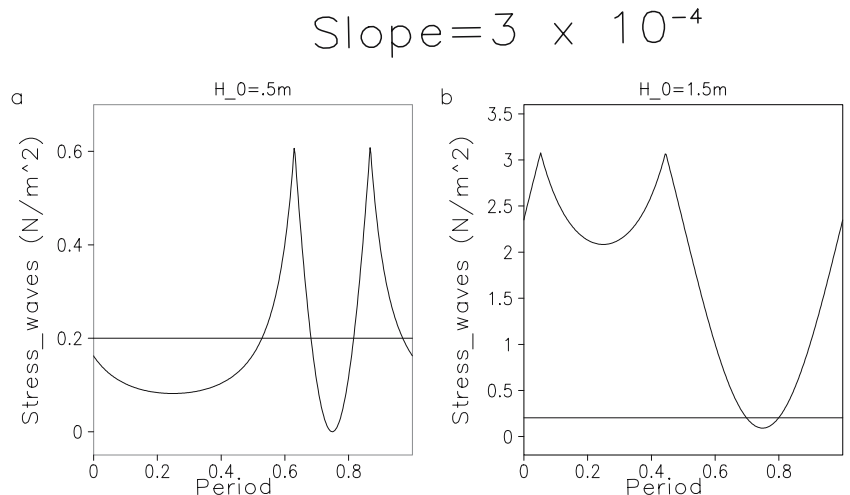
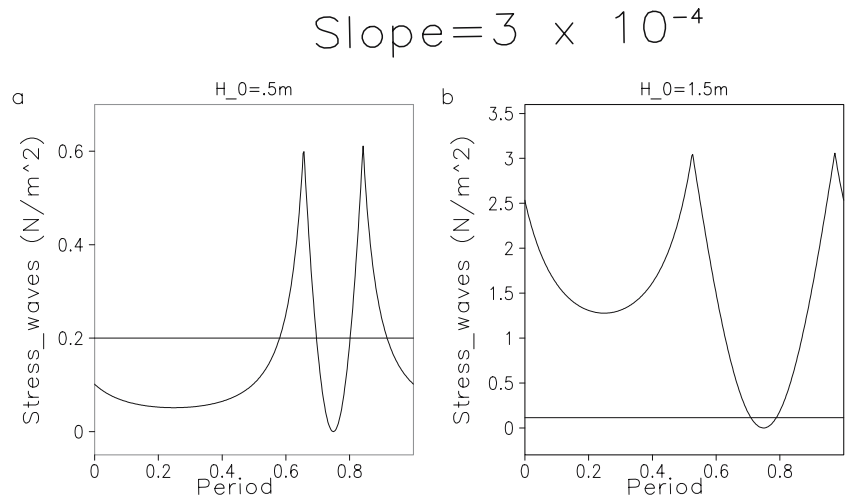




**Fig. 18** Temporal variability during one tidal period of bed shear stress due to wind waves. In this case  $f_w = 0.0031$  and the limiting factor  $(H/h)_{lim} = 0.8$ . The horizontal lines at  $0.2Nm^{-2}$  indicates critical shear stress



The importance of the limiting factor  $(H/h)_{lim}$  in Eq. 12 is revealed below from the comparison between Figs. 16, 17, and 18 in which  $(H/h)_{lim}$  is 0.15, 0.5, and 0.8, correspondingly. The friction factor in the first and third case is changed compared to the basic case (Fig. 17) in a way to ensure comparable magnitudes of bed shear stress. Obviously, beyond some values of  $(H/h)_{lim}$ , the temporal variability follows a similar pattern (compare Figs. 17 and 18), however, for small limiting factors such as those reported by Le Hir et al. (2000), the course of curves change substantially (some maxima disappear).

Following the simple model of Eq. 12 with  $(H/h)_{lim} = 0.5$  and  $f_w = 0.005$ , the bed shear stress at  $x = 0$  (local depth  $H_{LW}$ ) due to wind waves follows different patterns depending on the wave height (Fig. 17a,b). For small waves (Fig. 17a), the minimum stress occurs during low and high water. Both minima are lower than the critical value of  $0.2Nm^{-2}$ , thus enabling a deposition during these times. The temporal variability of bed shear stress due to high waves (Fig. 17b) reveals that only during low water are the values lower than the critical ones. Although there is a secondary minimum during high water, the corresponding values are too high to allow sedimentation. Thus, the total shear stress (Fig. 19b) demonstrates that depending on the wave height, favorable conditions for deposition (blue color) could occur two times per tidal period (for small waves) and one time for high waves. As seen in Fig. 19a, for waves with a constant height, the dependence of bed shear stress on the bottom slope is also very pronounced. For small slopes velocity is large and the bimodal oscillations are better pronounced. For relatively steeper bottom, the control of wind waves becomes dominant (the time of erosion decreases and that of deposition increases).

The above behavior of the bed shear stress due to breaking wind waves becomes clear if we express Eq. 11 as:

$$\tau_b^w = \frac{1}{8} \rho g f_w (H/h)_{lim} (h_0 + \zeta), \tag{25}$$

for small depths and

$$\tau_b^w = \frac{1}{8} \rho g f_w H_i^2 / (h_0 + \zeta), \tag{26}$$

for large depths where  $h_0$  is the mean depth. Thus, depending on the ratio between wind-wave magnitude and local depth,

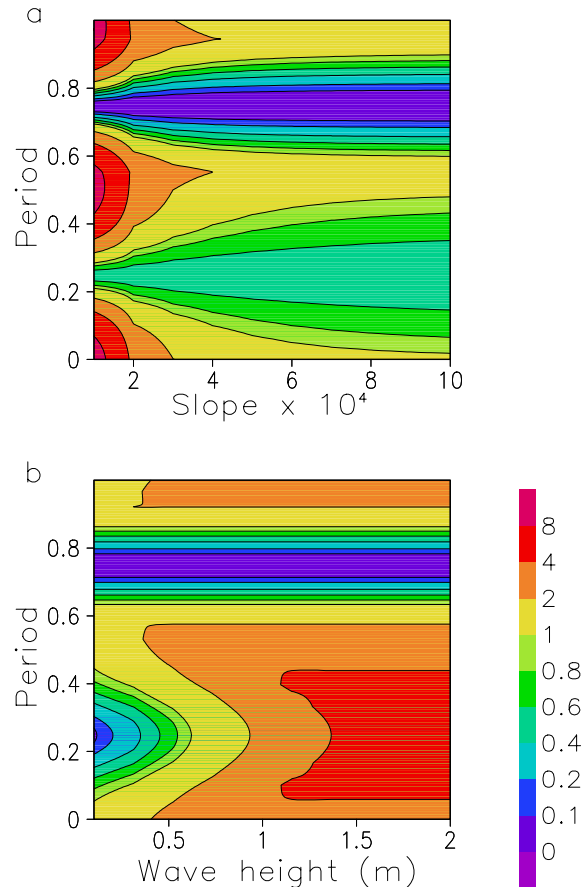


**Fig. 19** Bed shear stress ( $Nm^{-2}$ ) due to tides and wind waves. Time vs bottom slope diagram (a) and time vs wave height diagram (b). In this case,  $f_w = 0.005$  and the limiting factor  $(H/h)_{lim} = 0.5$

the control on bed shear stress is taken either by Eq. 25 or 26. The first case is clearly represented in Fig. 16d.

Because in the near-coastal zone  $\zeta$  reaches values that are comparable with the mean depth, the bed shear stress is expected to show a strong sensitivity to oscillations in sea level. Critical conditions (maximum in Fig. 3) are reached two times per tidal period. This is the reason for the bimodal oscillations of bed shear stress (Fig. 17). It is noteworthy that depending on the wave height, the “spikes” in the bed shear occur earlier for high waves and with some delay for the low wave heights. Therefore, there is an asymmetry of the response of bed shear stress to tidal forcing characterized with a pronounced spatial pattern.

## References

- Bruun P (1962) Sea level rise as a cause of shore erosion. *J Waterw Harb Div-ASCE* 88:117–130
- Bruun P (1978) Stability of tidal inlets. Theory and engineering. Developments in geotechnical engineering 23. Elsevier, Amsterdam, p 506
- Burchard H, Bolding K (2002) GETM—a general estuarine transport model. Scientific documentation, No EUR 20253 EN, European Commission, Italy, p 157
- Burchard H, Bolding K, Villareal MR (1999) GOTM—a general ocean turbulence model. Theory, implementation and test cases scientific documentation, No EUR 18745 EN, European Commission, Italy, p 103
- Clarke S, Elliot AJ (1998) Modelling suspended sediment concentrations in the firth of forth. *Estuar Coast Shelf Sci* 47:235–250
- Davies AM, Lawrence J (1994) Examining the influence of wind and wind wave turbulence on tidal currents, using a three-dimensional hydrodynamic model including wave-current interaction. *J Phys Oceanogr* 24:2441–2460
- Dick SK, Eckard K, Müller-Navarra SH, Klein H, Komo H (2001) The operational circulation model of BSH (BSHcmod)—model description and validation. *Berichte des Bundesamtes für Seeschifffahrt und Hydrographie* 29:49
- Dyer KR, Soulsby RL (1988) Sand transport on the continental shelf. *Annu Rev Fluid Mech* 20:295–324
- Einstein HA, Krone RB (1962) Experiments to determine modes of cohesive sediment transport in salt water. *J Geophys Res* 67:1451–1461
- Flemming BW (2002) Effects of climate and human interventions on the evolution of the Wadden Sea depositional system (Southern North Sea). In: Wefer G, Behre K-E, Jansen E (eds) *Climate development and history of the North Atlantic realm*. Springer, Berlin Heidelberg New York, pp 399–413
- Flemming BW, Davis RA (1994) Holocene evolution, morphodynamics and sedimentology of the Spiekeroog barrier island system (southern North Sea). *Senckenb Marit* 24:117–155
- Forbes DL, Orford JD, Taylor RB, Shaw J (1997) Interdecadal variation in shoreline recession on the Atlantic coast of Nova Scotia. In: *Proceedings of the Canadian coastal conference '97*, Guelph, Ontario. Canadian Coastal Science and Engineering Association, Ottawa, ON, Canada, pp 360–374
- Friedrichs CT, Aubrey DG, Speer PE (1990) Impact of relative sea-level rise on evolution of shallow estuaries. In: Cheng RT (ed) *Residual currents and long-term transport*. Springer, Berlin Heidelberg New York, pp 105–122
- Grant WD, Madsen OS (1979) Combined wave and current interaction with a rough bottom. *J Geophys Res* 84:1797–1808
- Jonsson IG (1966) Wave boundary layers and friction factors. In: *Proceedings of the 10th international conference on coastal engineering*, Tokyo, Japan, ASCE, pp 127–148
- Kaplin PA, Selivanov AO (1995) Recent coastal evolution of the Caspian Sea as a natural model for coastal responses to the possible acceleration of global sea-level rise. *Mar Geol* 124:161–175
- Komar PD, Enfield DB (1987) Short-term sea-level changes and coastal erosion. In: Nummedal D, Pilkey OH, Howard JD (eds) *Sea-level fluctuation and coastal evolution*. Society of Economic Paleontologists and Mineralogists, Tulsa OK, special publication no. 41, pp 17–27
- Krögel F, Flemming BW (1998) Evidence for temperature adjusted sediment distribution in the backbarrier tidal flats of the East Frisian Wadden Sea (southern North Sea). In: Alexander CR, Davis RA, Henry VJ (eds) *Tidalites: processes and products*, vol 61. SEPM Spec, pp 31–41
- Le Hir P, Roberts W, Caille O, Christie M, Bassoulet P, Bacher C (2000) Characterization of intertidal flat hydrodynamics. *Cont Shelf Res* 20:1433–1459
- Mehta AJ (1988) Laboratory studies on cohesive sediment deposition and erosion. In: Dronkers J, van Leussen W (eds) *Physical processes in estuaries*. Springer, Berlin Heidelberg New York, pp 327–345
- Nicholls RJ (1998) Assessing erosion of sandy beaches due to sea-level rise. In: Maund JG, Eddleston M (eds) *Geohazard in engineering geology*, vol 15. Engineering Geology Special Publications, Geological Society, London, United Kingdom, pp 71–76
- Partheniades E (1965) Erosion and deposition of cohesive soils. *Proc ASCE, J Hydraulics Div* 91:105–139
- Puls W, Sündermann J (1990) Simulation of suspended sediment dispersion in the North Sea. In: Cheng RT (ed) *Coastal and estuarine studies*, 38, Residual currents and long-term transport. Springer, Berlin Heidelberg New York
- Roberts WR, Le Hir P, Whitehouse RJS (2000) Investigation using simple mathematical models of the effect of tidal currents and waves on the profile shape of intertidal mudflats. *Cont Shelf Res* 20:1079–1097
- Rodi W (1980) Turbulence models and their application in hydraulics. Report Int Assoc Hydraul Res, Delft, Netherlands, p 104
- Santamarina Cuneo P, Flemming B (2000) Quantifying the concentration and flux of suspended particulate matter through a tidal inlet of the East Frisian Wadden Sea by acoustic Doppler current profiling. In: Flemming BW, Delafontaine MT, Liebezeit G (eds) *Muddy coast dynamics and resource management*. Elsevier Science, Amsterdam, The Netherlands, pp 39–52
- Schubert M, Blender R, Fraedrich K, Lunkeit F, Pertwitz J (1998) North Atlantic cyclones in CO<sub>2</sub>-induced warm climate simulations: frequency, intensity and tracks. *Clim Dyn* 14:827–837
- Signell RP, Beardsley RC, Graber HC, Capotondi A (1990) Effect of wave-current interaction on wind-driven circulation in narrow, shallow embayments. *J Geophys Res* 95:9671–9678
- Souza AJ, Simpson JH (1997) Controls on stratification in the Rhine ROFI system. *J Mar Syst* 12:311–323
- Stanev EV, Flöser G, Wolff J-O (2003a) Dynamical control on water exchanges between tidal basins and the open ocean. A Case Study for the East Frisian Wadden Sea. *Ocean Dynamics* 53:146–165
- Stanev EV, Wolff J-O, Burchard H, Bolding K, Flöser G (2003b) On the circulation in the East Frisian Wadden Sea: numerical modeling and data analysis. *Ocean Dynamics* 53:27–51
- The WASA Group (1998) Changing waves and storms in the Northeast Atlantic? *Bull Am Meteorol Soc* 79(5):741–760 (May 1998)
- van der Molen J, de Swart HE (2001) Holocene wave conditions and wave-induced sand transport in the Southern North Sea. *Cont Shelf Res* 21:1723–1749
- van Leussen W (1988) Aggregation of particles, settling velocity of mud flocks. In: Dronkers J, van Leussen W (eds) *Physical processes in estuaries*. Springer, Berlin Heidelberg New York, pp 347–404